Geophysical Research Letters

RESEARCH LETTER
10.1029/2020GL087504

Enhanced North American ENSO Teleconnections During the Little Ice Age Revealed by Paleoclimate Data Assimilation

Sylvia Dee[1], Yuko Okumura[2], Samantha Stevenson[3], and Pedro Di Nezio[2]

[1]Department of Earth, Environmental, and Planetary Sciences, William Marsh Rice University, Houston, TX, USA, [2]Institute for Geophysics, Jackson School of Geosciences, University of Texas at Austin, Austin, TX, USA, [3]Bren School of Environmental Sciences & Management, University of California, Santa Barbara, CA, USA

Abstract Teleconnection rainfall over North America may be systematically altered by tropical Pacific mean state changes. Characterizing teleconnection changes to improve prediction requires many realizations of ENSO events, but twentieth century data are temporally limited. To extend twentieth century records, we evaluate ENSO events in a new last-millennium paleoclimate data assimilation reconstruction to deduce how mean state changes affect the magnitude/extent of ENSO-driven rainfall in the United States. Despite global cooling during the Little Ice Age, the central-eastern tropical Pacific warms relative to the Medieval Climate Anomaly, shifting teleconnections eastward and increasing rainfall anomalies in the southwestern United States. Teleconnections strengthen independently of ENSO amplitude; we thus suggest caution in using paleoclimate reconstructions of teleconnection rainfall as a proxy for ENSO amplitude. We demonstrate teleconnection rainfall is sensitive to the pattern of tropical Pacific mean SST changes, underscoring the importance of reducing uncertainties in future warming patterns in the tropical Pacific.

Plain Language Summary As we accelerate into a future with higher greenhouse gas concentrations, it is critical to constrain how the El Niño–Southern Oscillation (ENSO)—arguably the most influential driver of weather and climate on Earth—will change. There are still large unknowns surrounding how the tropical Pacific will respond to anthropogenic changes in greenhouse gas concentrations, as well as its associated impacts on rainfall in midlatitude regions such as the United States. Here, we investigate how ENSO and its relationship to rainfall respond to changes in Earth's "average" climate in the past. We explore two key periods during the last millennium in data generated using a new technique called paleoclimate data assimilation. This fuses the information in paleoclimate archives, such as tree rings and corals, with the physics of the atmosphere and ocean represented in global climate models. We examine annually resolved climate "snapshots" and find that changes in U.S. rainfall are acutely sensitive to changing tropical Pacific sea surface temperature patterns. These patterns have important similarities with predictions of global warming in 2100. Analogs from time periods in Earth's past with very different mean climate highlight the importance of reducing uncertainties in future warming patterns in the tropical Pacific for rainfall prediction.

Key Points:
- ENSO and teleconnection rainfall sensitivity to mean state changes in climate is evaluated in the Last Millennium Reanalysis
- Teleconnection rainfall in the United States is enhanced during the Little Ice Age compared to the Medieval Climate Anomaly
- Rainfall sensitivity to SST warming patterns underscores the importance of reducing spatial SST uncertainties in global warming scenarios

Supporting Information:
- Supporting Information S1

Correspondence to:
S. Dee,
sylvia.dee@rice.edu

Citation:
Dee, S., Okumura, Y., Stevenson, S., & Di Nezio, P. (2020). Enhanced North American ENSO teleconnections during the Little Ice Age revealed by paleoclimate data assimilation. *Geophysical Research Letters*, *47*, e2020GL087504. https://doi.org/10.1029/2020GL087504

Received 13 FEB 2020
Accepted 15 JUN 2020
Accepted article online 8 JUL 2020

1. Introduction

Year-to-year variations in sea surface temperatures (SSTs) over the tropical Pacific exert a large influence on global weather and climate. These variations are driven by the El Niño–Southern Oscillation (ENSO) phenomenon (Philander, 1989), which in turn impacts the global atmosphere by forcing stationary Rossby waves and altering the zonal-mean atmospheric circulation (Alexander et al., 2002; Trenberth et al., 1998). The subtropical jet stream and associated storm tracks move southward during El Niño—the warm phase of ENSO—and northward during La Niña—the cold phase. These circulation changes, also known as "teleconnection" patterns, result in pronounced seasonal changes in U.S. rainfall. The characteristics and dynamics of ENSO teleconnections are documented in both historical observations (Alexander et al., 2002; Hoerling & Kumar, 1997; Hoerling et al., 1997; Horel & Wallace, 1981; Seager et al., 2003; Ting & Hoerling, 1993; Trenberth et al., 1998, and many others) and model simulations (Deser et al., 2017; Hoell et al., 2016; Lloyd et al., 2009, 2011, 2012).

ENSO teleconnections may be sensitive to changes in mean climate. In the context of greenhouse gas (GHG) forcing (e.g., Stevenson, 2012; Zheng et al., 2016), several studies have found that when the tropical Pacific warms more in the east than in the west, tropical precipitation anomalies forcing stationary waves tend to shift eastward (Bonfils et al., 2015; Zhou et al., 2014). Many climate models and some observational evidence suggest a weakened Walker circulation and enhanced equatorial warming with a slight decrease in the east-west SST gradient in response to greenhouse gas forcing (e.g., Cai et al., 2015; Collins et al., 2010; DiNezio et al., 2009; Held & Soden, 2006; Tierney et al., 2019; Tokinaga et al., 2012; Vecchi et al., 2006; Xie et al., 2010), consistent with the multimodel mean response in the Coupled Model Intercomparison Project (CMIP) Phases 3 and 5 (Cai et al., 2015; Collins et al., 2010; Stevenson et al., 2012). Additionally, while the magnitude of El Niño events themselves show little to no change in climate model projections spanning the 21st century, a mean eastward shift in ENSO teleconnection-driven precipitation anomalies, particularly over the United States, is observed in many CMIP class projections (Stevenson, 2012; Stevenson et al., 2012; Zhou et al., 2014). However, this El Niño-like mean state response of the tropical Pacific to GHG forcing is still the subject of considerable debate due to uncertainties in observations, mechanisms, and climate model simulations (e.g., Coats & Karnauskas, 2017; Deser et al., 2010; DiNezio et al., 2010; Karnauskas et al., 2009; Seager et al., 2019; Solomon & Newman, 2012; Vecchi et al., 2008).

Thus, historical observations are inconclusive regarding the pattern of future mean SST changes and associated shifts in ENSO teleconnections. Previous studies rely heavily on twentieth century observations, which span approximately 22 La Niña and 26 El Niño events (NOAA, 2017) over the last 70 years (Coats & Karnauskas, 2017; Deser et al., 2017; Frauen et al., 2014; Garfinkel et al., 2013; Hoerling et al., 2001; Horel & Wallace, 1981). This paucity of historical data may not be sufficient to fully isolate the impact of tropical SSTs on midlatitude variability, and modeling studies have previously shown that atmospheric teleconnections are highly variable (Coats et al., 2013; Coats & Karnauskas, 2017; Deser et al., 2017; Stevenson et al., 2015). This highlights the need for additional data to extend the length of the observational record.

High-resolution paleoclimate archives from the past 1,000 years (the Last Millennium, LM hereafter) are an essential source of information to augment the instrumental record. Such data have previously been used to assess ENSO teleconnection changes (Goosse et al., 2012; Kaufman et al., 2009). Of particular interest are the Little Ice Age (LIA), thought to have relatively cold global temperatures, and the Medieval Climate Anomaly (MCA), when North Atlantic temperatures were warmer. These periods have been used extensively as targets for LM climate field reconstruction (e.g., Wang et al., 2015), and climate changes from the MCA to LIA are well documented (Emile-Geay et al., 2013a; Graham et al., 2011; Henke et al., 2017; Hereid et al., 2013; Lawman et al., 2019; Li et al., 2011; Loisel et al., 2017; Mann et al., 2009; McGregor et al., 2013; Wang et al., 2015). Several LM reconstructions indicate a persistent "La Niña-like" mean state during the MCA with a strengthened tropical Pacific SST gradient (Cobb et al., 2003; Cook et al., 2010; Herweijer et al., 2006, 2007; Mann et al., 2009; Newton et al., 2006; Rustic et al., 2015; Seager et al., 2007; Trouet et al., 2009), invoking forcing via the dynamical thermostat mechanism (Clement et al., 1996). More recent literature suggests that a cooler tropical Pacific mean state during the MCA results from internal variability, generating multidecadal periods containing a relatively high number of La Niña events (Ault et al., 2018; Coats et al., 2016, 2016; Steiger et al., 2019). The robustness of MCA-LIA differences in proxy reconstructions has been questioned in the past, with issues arising due internal variability and/or reconstruction methodology (e.g., Emile-Geay et al., 2013c; Henke et al., 2017; Smerdon et al., 2016; Wang et al., 2015). Nevertheless, data spanning the LIA and MCA provide a useful test for the hypothesis that long-term changes in mean climate modulate ENSO teleconnections (Goosse et al., 2012; Kaufman et al., 2009; Masson-Delmotte et al., 2013).

However, the limited spatial extent of paleoclimate reconstructions information limits their capacity to yield dynamical inferences. Addressing this, the recent acceleration of research employing paleoclimate data assimilation (DA) to reconstruct past climates has broadened existing climate field reconstruction techniques by fusing the information contained in paleoclimate records with the dynamics of climate models (Brönnimann et al., 2013; Franke et al., 2017, 2020; Goosse et al., 2010; Hakim et al., 2013; Steiger et al., 2014, 2018; Widmann et al., 2010). Among these efforts is the Last Millennium Reanalysis, or LMR (Hakim et al., 2016; Tardif et al., 2019), which yields temperature, precipitation, sea level pressure, and geopotential height anomalies during the full LM. This allows dynamical hypotheses regarding ENSO teleconnection changes to be more rigorously tested in a dynamically consistent framework constrained by paleoclimate information.

Here we present the first application of the LMR to variations in ENSO teleconnections over the past millennium. In particular, we capitalize on the fact that there are subtle mean state changes in the tropical Pacific during the LM that can be used to study how ENSO teleconnections respond to such small changes in mean state. Future changes in Pacific mean state are also expected to be subtle, but their effect on teleconnections remains uncertain. Furthermore, quantifying the sensitivity of ENSO teleconnections to changes in mean state is likely to bolster our ability to assess the accuracy of future model projections.

2. Data and Methods

2.1. Paleoclimate and Model Data

This study relies on the Last Millennium Reanalysis Project V2.0 (see Hakim et al., 2016; Tardif et al., 2019, for a full description of the data product) (supporting information sections S1 and S2). The LMR uses offline DA using a prior derived from climate model simulations spanning the last millennium (Landrum et al., 2013) and annually resolved paleoclimate archives from the PAGES2k database (PAGES2K Consortium, 2013) (with later additions from (Anderson et al., 2019; Tardif et al., 2019)). The DA employs an ensemble Kalman filter to reconstruct annual climate states which minimize the offset between model fields (the model "prior") and observations (Hakim et al., 2016; Steiger et al., 2013; Tardif et al., 2019). The result is an annually resolved reconstruction of fields including (but not limited to) SST, surface temperature, precipitation, the Palmer Drought Severity Index (PDSI), and geopotential height. All fields are reconstructed as annual anomalies from the 1951–1980 mean. The characteristics of ENSO in the LMR are validated in supporting information section S2 (Figures S1 and S2 Kennedy et al., 2011; Percival & Walden, 1993).

We note that paleoclimate proxies assimilated into the LMR contain seasonal biases, dating errors, and that the data availability decreases back in time, causing variance loss in the reconstruction mean (Hakim et al., 2016; Tardif et al., 2019). The LMR also reconstructs calendar year anomalies (January–December), which likely splits the peak seasonal ENSO impact across calendar years, and restricts our ability to assess monthly seasonal scale rainfall variability. Nonetheless, the LMR provides a complement to direct measurements from paleoclimate archives, as it effectively fuses information contained in the high-resolution paleoclimate record with the dynamical constraints of a climate model (Dee et al., 2016; Steiger et al., 2013); the LMR thus "fills in the gaps" in time and space where data points are lacking in the paleoclimate record (Hakim et al., 2016; Tardif et al., 2019). The output contains 20 Monte Carlo (MC) iterations generated via randomly sampling 75% of the available proxy data and using different draws from the climate model ensemble priors in the assimilation (see supporting information sections S1, and S9 for an evaluation of the impact of the LMR model prior on our analysis). We focus on the ensemble and Monte Carlo iteration mean, using the spread in the MC iterations for uncertainty quantification.

2.2. Definitions

We adopt the methodology employed in Seager et al. (2008) to select the MCA and LIA as key time periods in the LM. The MCA is defined here as the period from 950 to 1350 CE, and the LIA is defined as 1400–1800 CE.

These periods are chosen due to the high volume of research into both the timing of and climatic forcings causing these two large mean state changes in global temperature, potentially affecting ENSO teleconnections (Clement et al., 1996; Cobb et al., 2003; Emile-Geay et al., 2013b, 2013c; Graham et al., 2011; Henke et al., 2017; Lawman et al., 2019; Mann et al., 2009; McGregor et al., 2013; Phipps et al., 2013; Wang et al., 2013).

El Niño and La Niña events are defined independently in the LMR via averaging the reconstructed SST field over the NINO3.4 region (5°N to 5°S, 170–120°W) during both the MCA and LIA. We extract El Niño and La Niña events as departures exceeding $\pm 1\sigma$ of NINO3.4 SST anomalies (defined as deviations from SST climatology for the reference period, LIA or MCA). This yields approximately 120 ENSO events, ~60 El Niño and ~60 La Niña for both the LIA and MCA, with an average return period of 7 years. Teleconnection patterns are computed by compositing departures from the LIA and MCA climatology for the variable of interest (in this case, precipitation or PDSI) for all El Niño and La Niña events during the respective periods (as in Rasmusson & Carpenter, 1982; Rasmusson & Wallace, 1983; Ropelewski & Halpert, 1986). Precipitation is normalized by the standard deviation (1σ) of the NINO34 index over the period of interest (i.e., LIA and MCA) to remove the impact of ENSO amplitude (following the methodology of Stevenson, 2012). This

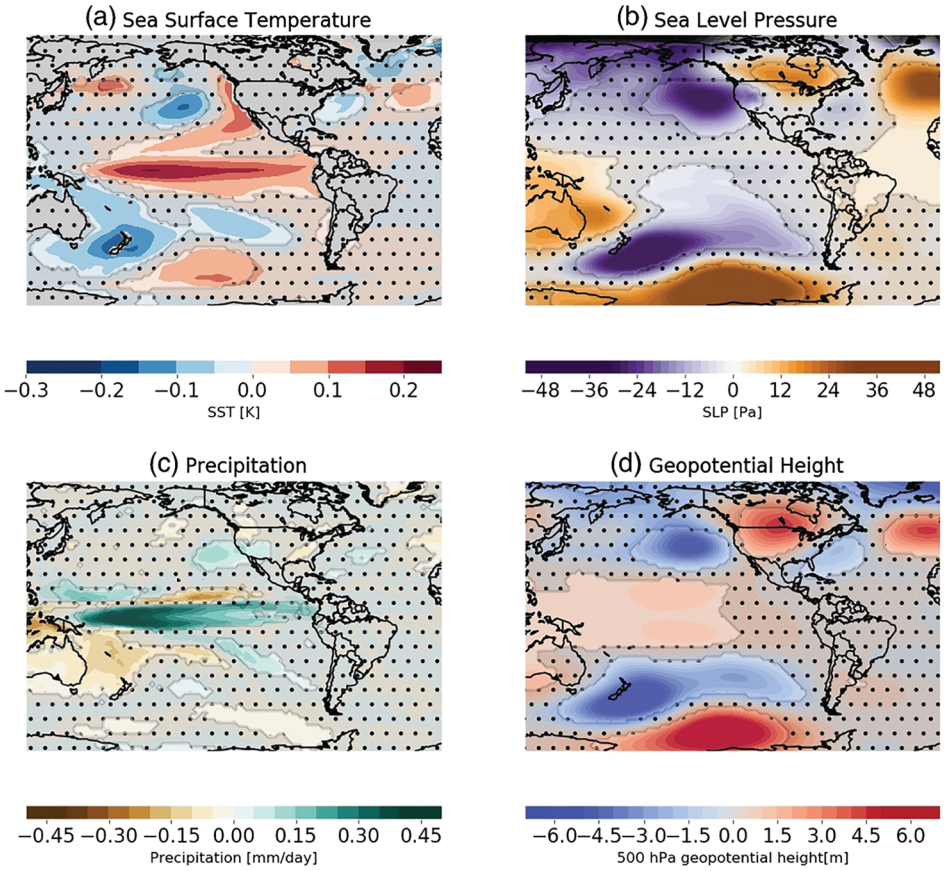

Figure 1. LMR mean state differences, LIA minus MCA. (a) surface temperatures (K), (b) sea level pressure (Pa), (c) precipitation rate (mm/day), and (d) 500 hPa geopotential height (m). Stippling and shading indicates insignificant (p>0.05) result of two-tailed t test on the MC runs.

treatment captures changes in moisture supply in teleconnected regions during ENSO events in different mean climates. ENSO amplitude is defined as the value of the standard deviation of the relevant index (NINO3, NINO4, or NINO3.4).

3. Results

3.1. ENSO and Mean State Changes

We first examine changes in the mean state and ENSO amplitude between the MCA and LIA. Table S1 and Figure S3 compare the mean ENSO amplitude for the NINO3, NINO34, and NINO4 regions during these periods for the LMR, as well as the mean SST anomaly in each region. To test for statistical significance, we evaluated the 1σ spread for the 20-member MC reconstruction output. ENSO amplitude is not significantly different (two-tailed Student's t test) during the LIA compared to the MCA in the NINO3.4 or NINO3 region; in the NINO4 region, further west, variance is higher during the MCA (0.26°C) compared to the LIA (0.21°C) (significantly different at the 95% confidence level). In general, we observe minimal changes in ENSO amplitude, with differences in 1σ values on the order of 0.01–0.05 K. Much larger changes on centennial timescales are known to be possible given internal variability (Stevenson et al., 2012; Wittenberg, 2009). We therefore conclude that there is a lack of robust evidence for a significant change in ENSO amplitude between the MCA and LIA.

The changes in tropical climate during the LIA relative to the MCA show features characteristic of an altered east-west SST gradient, associated shifts in tropical rainfall, and extra tropical changes over North America. Mean temperatures in both the central and eastern equatorial Pacific are warmer during the LIA compared to the MCA (Figure 1a and Table S1, mean SST anomalies). This “El Niño-like” warming pattern is

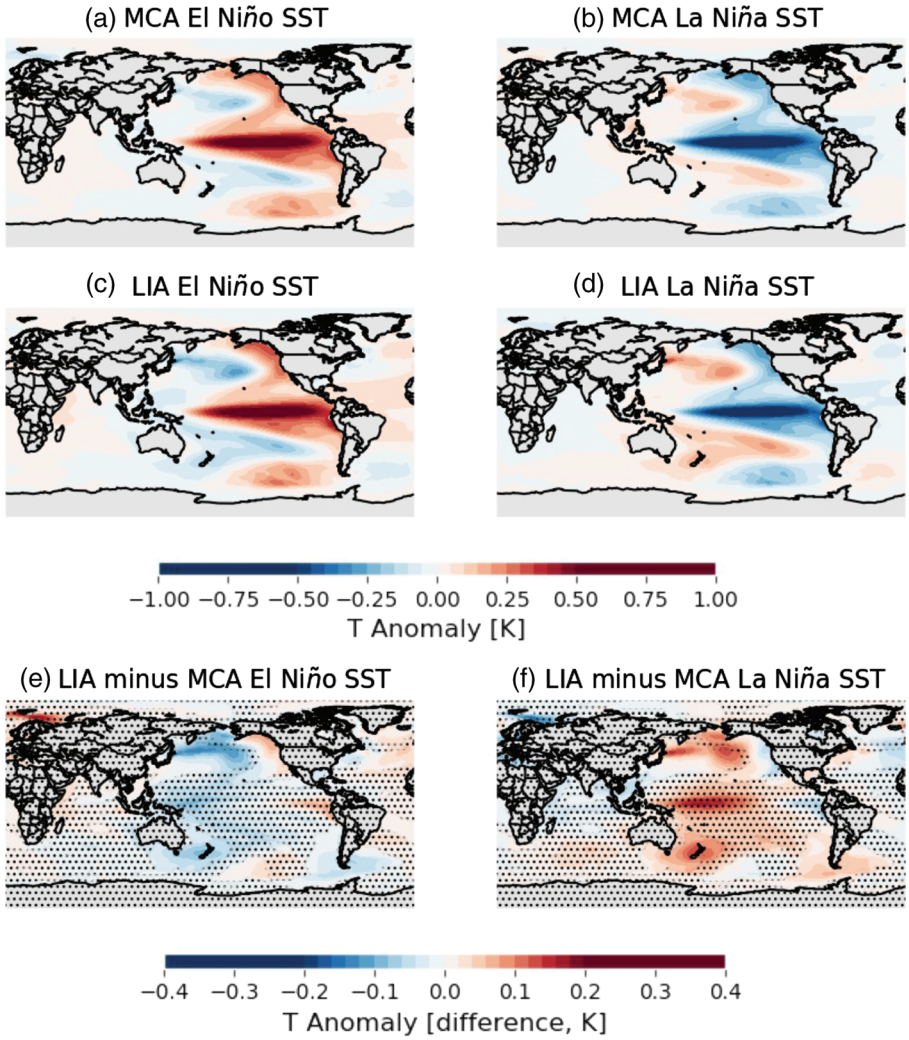

Figure 2. Change in El Niño and La Niña SST for the LIA and MCA in the LMR (a) MCA El Niño SST, (b) MCA La Niña SST, (c) LIA El Niño SST, (d) LIA La Niña SST, (e) LIA minus MCA El Niño, and (f) La Niña SST anomalies (temperature, Kelvin); stippling indicates SST changes are not significant ($p>0.05$, two-tailed t test of the 20-member LMR MC iterations). Note that the color bar scale is different in the bottom two panels showing the SST anomaly differences (LIA-MCA) rather than the composite anomalies.

consistent with previous work suggesting radiatively forced "La Niña-like" mean state changes in the MCA relative to the LIA (Cobb et al., 2003; Cook et al., 2010; Herweijer et al., 2006, 2007; Mann et al., 2009; Newton et al., 2006; Rustic et al., 2015; Seager et al., 2007; Trouet et al., 2009). The center of maximum SST variance shifts eastward in the tropical Pacific during the LIA, coupled with reduced SST variance in the western tropical Pacific (Figure S4). This is also evident in the NINO4 changes in MCA versus LIA variance, which is significantly reduced in the western tropical Pacific during the LIA. LIA minus MCA changes in precipitation exhibit an El Niño-like pattern with increased central and eastern tropical Pacific rainfall anomalies, accompanied by a deepening of the Aleutian low (Figures 1c and 1d).

Overall, Figures 1 and S4 are suggestive of a change in ENSO driven by MCA-LIA mean climate differences, despite the lack of significant change in ENSO amplitude. Figure 2 shows the MCA and LIA El Niño and La Niña SST anomaly composites, indicative of a change in ENSO diversity between the two periods. El Niño events show an eastward shift of warm SST anomalies during the LIA (Figure 2e). However, these LIA-MCA changes across the tropics are not significant (two-tailed t test, $p>0.05$). Finally, while the pattern of extratropical SST anomalies does not change substantially between the LIA and MCA, the amplitude is increased during LIA.

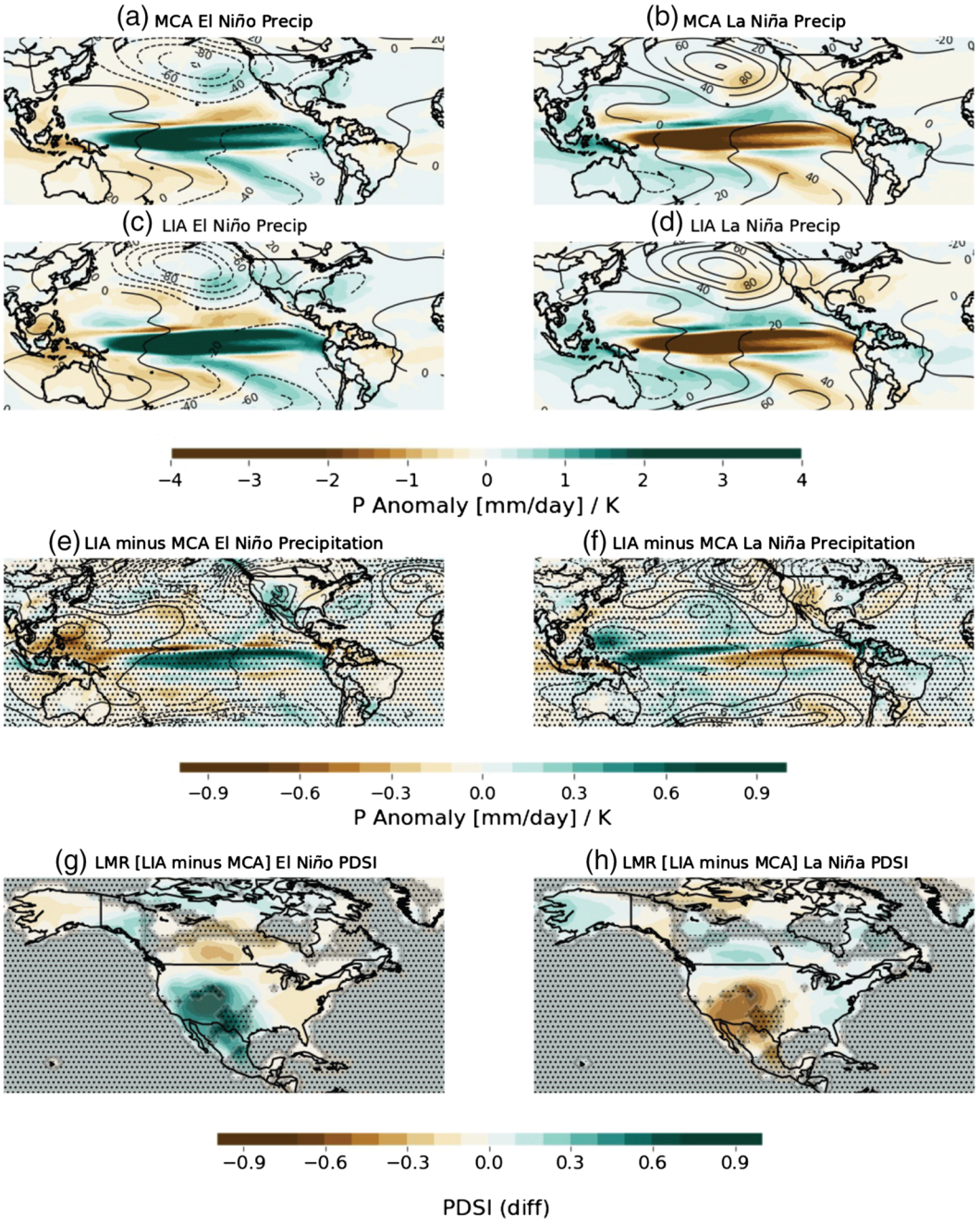

Figure 3. Changes in El Niño and La Niña precipitation (color scale) and SLP (contours) for the LIA and MCA based on the LMR. El Niño precipitation (mm/day·K^{-1}) (shading; scaled to NINO3.4 1σ for the respective time period); and SLP (contours at intervals of 20 Pa) anomalies during (a) MCA, (c) LIA, and (e) and their difference (LIA minus MCA). (b, d, f) As in (a), (c), and (e) but for La Niña. (g, h) As in (e) and (f) but for PDSI anomalies (unitless) over North America. Note that the color bar scale is different in the bottom four panels (e)–(h), which show difference maps (LIA-MCA) as opposed to ENSO composites in (a)–(d).

3.2. ENSO Teleconnection Changes

We next analyzed the spatial signature of changes in El Niño and La Niña hydroclimate anomalies. Figure 3 shows the precipitation, sea level pressure (SLP), and Palmer Drought Severity Index (PDSI) anomalies for El Niño and La Niña events during the MCA and LIA.

During the LIA, ENSO teleconnections over North America are strengthened: El Niño-driven rainfall is enhanced in the Southwest, with wetter conditions stretching from California throughout the Southwest and Mexico (and see Figure S5 same results, zoomed in over the United States). Moisture supply is enhanced during El Niño and reduced during La Niña; the magnitude of moisture supply changes rather than the rainfall patterns as evidenced by the consistent patterns shown in Figure S5. During the LIA, La Niña events exhibit drier anomalies (Figures 3f and 3h), especially across the Southwest and Central Plains. A two-tailed *t* test across the MC iterations of the ensemble indicates western U.S. and east coast changes are significant at the 95% level. Changes in PDSI (LIA minus MCA) are also significant at the 95% level for most areas of the United States, with the exception of Texas and parts of the central Rocky Mountains (Figures 3g and 3h).

We next analyzed probability density functions for the U.S. Southwest (30°N to 43°N, 245°E to 253°E) and California (33°N to 42°N, 122°W to 115°W) rainfall and PDSI during La Niña and El Niño events for both the MCA and LIA (Figures S6 and S7). Both regions have recently experienced severe drought and unpredictable heavy rainfall events (Hoell et al., 2016). For the LMR, in both regions, El Niño PDSI is higher (indicating wetter conditions) during the LIA than during the MCA. Consistent with the rainfall anomalies in Figure 3, in both regions, La Niña PDSI decreases during the LIA compared to the MCA. Taken together, the LMR reconstruction results suggest the North American ENSO teleconnection was stronger during the LIA than during the MCA.

Both El Niño and La Niña precipitation anomalies are enhanced over the central-eastern equatorial Pacific during the LIA. The enhancement is likely due to the eastward shift of El Niño and La Niña SST anomalies (Figures 2e and 2f) and increased mean SST/convection in the central eastern equatorial Pacific (Figures 1a and 1c.) during the LIA. Eastern Pacific warming may increase the sensitivity of precipitation to ENSO SST anomalies, as described in Bonfils et al. (2015), Johnson and Xie (2010), and Power et al. (2013). The mean state warming pattern shown in Figure 1a. likely plays a more important role than ENSO SST changes, which are not statistically significant (Figures 2e and 2f, stippled pattern). The enhanced equatorial precipitation anomalies are likely to force stronger ENSO teleconnection and enhance atmospheric circulation anomalies over the eastern North Pacific in Figure 3, and these changes in the ENSO teleconnection occur in absence of significant changes in ENSO amplitude.

The intensification of hydroclimate teleconnections during the LIA is reflected in circulation anomaly changes as well. Figure 3 indicates amplified low pressure anomalies in the eastern North Pacific during the LIA El Niño (Figure 3e), which likely enhance subtropical westerly moisture transport to the U.S. Southwest. The LIA SLP anomalies show enhanced high pressure anomalies over the North Pacific during La Niña events (Figure 3f), known to exacerbate dry conditions across the U.S. Southwest.

For completeness, we repeated our analysis using an alternative teleconnection definition, and computed one-sided regression maps (Hoerling et al., 2001) for NINO34 SSTs and the dynamical fields of interest (precipitation and geopotential height) (e.g., Wallace & Gutzler, 1981 and many others). Our results are consistent across both teleconnection definitions; the regression coefficients for positive NINO34 index (Figure S8) and negative NINO34 index (Figure S9) events and rainfall strengthen during the LIA over the U.S. Southwest (Figures S8c and S9c). Furthermore, Figures S8 and S9 show the geopotential height regression coefficients increase (in absolute value) during the LIA, especially over the North Pacific and northern North America, indicative of increased teleconnection amplitude. This intensified teleconnection pattern amplifies both El Niño and La Niña hydroclimate anomalies (Figure 3), though the effect is more pronounced for El Niño events. Spatial patterns in rainfall remain consistent, ruling out a spatial shift in the teleconnection (Figure S5). These results confirm precipitation is more sensitive to changes in NINO34 SSTs during the LIA.

As a final sensitivity test, we performed the same analysis on a DA reconstruction which uses a fixed proxy network spanning 850–2000 CE (see Parsons & Hakim, 2019) (section S6). As described in Emile-Geay et al. (2017) and Hakim et al. (2016), the number of proxy records assimilated into the reconstruction varies over the last 2000 years, with proxy density increasing over time. Changing data availability with time can lead to spurious changes in either mean or variance in the reconstructions. Testing for this directly, Figure S10 shows that the enhanced teleconnection rainfall result holds for a sensitivity test which uses fixed proxy availability for 850 CE. We conclude that the teleconnection response pattern is robust to changes in

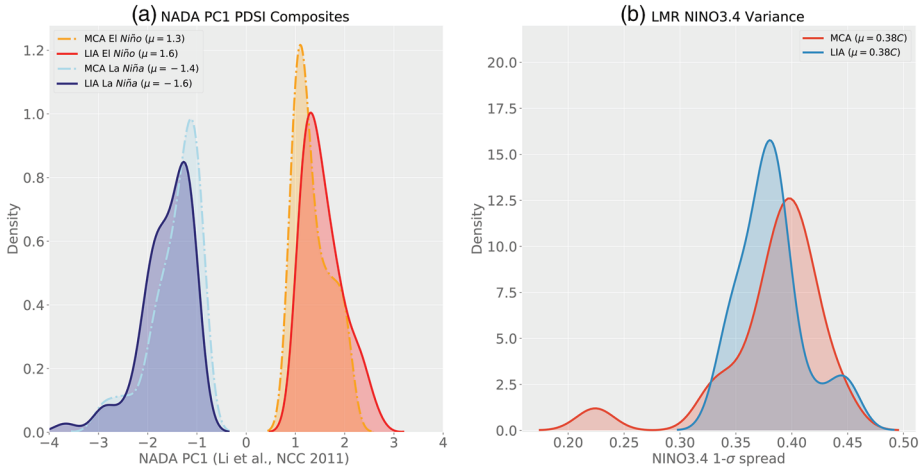

Figure 4. Comparison of NADA to LMR LM Teleconnections. (a) PDFs of the NADA PC1 (Li et al., 2011) for wetter (interpreted as El Niño) and drier (interpreted as La Niña) event composites during MCA (orange and light blue, dashed curves) and LIA (red and dark blue, solid curves). Wet (El Niño) and dry (La Niña) events are defined by PC1 excursions exceeding $\pm 1\sigma$, where σ is time period dependent. The means of the distributions are shown in the figure legend. The distributions for dry events are significantly different at the 90% confidence level (p=0.06) per a two-tailed t test, and for wet events, significantly different at the 95% confidence level (p=0.002). The number of events for each PDF: LIA El Niño = 63, MCA El Niño = 62; LIA La Niña = 65, MCA La Niña =66. (b) Reconstructed ENSO amplitude (1σ) for the NINO34 index in the LMR. The PDF represents the spread in the standard deviation (σ) for the 20 MC iterations of the LMR. The full ensemble mean values for all indices are given in Table S1. The 1σ values for the ensemble of MC realizations are shown for the LIA (blue line) and MCA (red line).

proxy availability over time, albeit with changes in the significance of the result due to a smaller ensemble size.

3.3. Comparison to Tree Ring Reconstructions

To check the LMR-based estimates of changes in ENSO teleconnection rainfall against a complementary data source derived from paleoclimate proxies alone (without the use of DA), we evaluated PDSI reconstructions from the North American Drought Atlas (NADA) (Cook et al., 2004, 2014), which relies exclusively on tree ring widths. Specifically, we evaluated changes in the first principal component (PC1) of the NADA from Li, Xie, et al. (2011), which primarily isolates hydroclimate changes in the Southwest United States; the record is also highly correlated to ENSO over the instrumental period.

Figure 4a shows the PDFs for PC1 excursions exceeding $\pm 1\sigma$, interpreted as hydroclimate variance due to ENSO teleconnection rainfall. Changes in hydroclimate are compared for the MCA and LIA; here, for consistency we use El Niño and La Niña to label the wet versus dry periods, respectively. The variance in the NADA PC1 is slightly reduced during the MCA (0.92) compared to the LIA (1.0). Similarly to the LMR, the NADA PC1 indicates a shift toward wetter conditions for El Niño events during the LIA (red curve), and drier conditions during La Niña (navy curve) compared to the MCA (orange, light blue curves). Changes for both ENSO phases significant at the 90% confidence level. Taken together, this suggests a strengthened teleconnection alongside increased hydroclimate variability during the LIA in NADA.

A number of paleoclimate reconstruction studies have historically related the strength of the midlatitude hydroclimate variabilty to ENSO amplitude (e.g., D'Arrigo et al., 2005; Li, Nakatsuka, et al., 2011; Li, Xie, et al., 2011; Loisel et al., 2017, and many others). While the *pattern* of SST variance changes (as mentioned above, Figure S4c), features enhanced variance in the east and reduced variance in the west, Table S1 and Figure 4b confirm that there is no significant change in NINO3.4 or NINO3 SST amplitudes for the LIA versus the MCA (and see Figure S3). Moreover, NINO4 amplitudes are reduced during the LIA. These findings suggest that directly tying teleconnection strength to ENSO amplitude may be misleading: teleconnection strength can change independently of ENSO variability, and the centroid of that variability matters. The NADA PC1 is a record of changes in moisture supply, but does not necessarily reflect ENSO variability.

Such a conclusion would require a stable teleconnection with the tropical Pacific, but we assert the teleconnection is not stable over the full LM, and depends acutely on the pattern of SST change over time. ENSO rainfall may be altered by the pattern of tropical Pacific warming, and these patterns are not necessarily tied to ENSO amplitude.

4. Discussion and Conclusions

This study demonstrates that changes in tropical Pacific mean state can drive shifts in ENSO rainfall patterns, in the absence of changes in ENSO amplitude. The LIA minus MCA SST changes in the LMR agree with previous work suggesting a "La Niña-like," radiatively forced mean state change during the MCA relative to the LIA (Cobb et al., 2003; Cook et al., 2010; Herweijer et al., 2006, 2007; Mann et al., 2009; Newton et al., 2006; Rustic et al., 2015; Seager et al., 2007; Trouet et al., 2009). We find that ENSO teleconnections strengthened during the LIA relative to the MCA, likely due to warmer mean SSTs in the central and eastern tropical Pacific shifting the locus of tropical Pacific convection anomalies to the east, enhancing rainfall over North America. This result holds for both El Niño and La Niña events: there is less drying in the Southwest during MCA La Niña events. However, there is little evidence for a change in the amplitude of ENSO-related SST anomalies; rather, we find that moisture supply is sensitive to changes in the pattern of SST warming during the LIA. The use of proxies from ENSO-teleconnected regions to reconstruct ENSO amplitude thus houses considerable uncertainties. The analysis of the NADA in this context serves as a complementary analysis, and we suggest caution interpreting teleconnection changes as a direct proxy for tropical Pacific SST variance. While the LMR is not a perfect representation of reality, it does provide a dynamically consistent, spatiotemporally gridded field housing both SST and rainfall, yielding insight into the patterns and dynamics operating in the LM in a way that other paleoclimate data products cannot. Expanding high-fidelity paleoclimate archives of SST changes (e.g., from coral oxygen isotopic records) would bolster ENSO amplitude reconstructions over the last several centuries (Cobb et al., 2003; Dee et al., 2020; Russon et al., 2015; Stevenson et al., 2012; Tierney et al., 2015).

Our results highlight large uncertainties in reconstructing both ENSO amplitude and teleconnection patterns from proxies in teleconnected regions, in agreement with recent studies (e.g., Abram et al., 2020). A primary advantage here is that the LMR does not house assumptions surrounding teleconnection stationarity common to regression-based CFR methods. However, we acknowledge the LMR explicitly relies on teleconnections via covariance assumptions supplied by the model, instead of defined covariance patterns in a calibration interval. Thus, because the enhanced ENSO teleconnection during LIA observed in the LMR is constrained by tree ring records, it is difficult to deduce the skill in the reconstruction for both ENSO amplitude and the pattern of ENSO during the MCA and LIA. While a number of rich, highly resolved coral records are assimilated across the tropical Pacific, few coral records span both the MCA and LIA in full, and are not assimilated to the LMR. We acknowledge that these uncertainties may affect our results, given that the proxy availability during the MCA and LIA is not identical. To address this, we confirmed that our results are robust to changes in proxy availability (Figure S10) by assimilating a subset of proxy records, rather than the full PAGES2k data set.

Finally, there are significant LIA-MCA differences in midlatitude (e.g., North Pacific) SST anomalies during El Niño and La Niña (Figures 2e and 2f), which likely result from different tropical forcing, but may in turn alter the ENSO teleconnection downstream (e.g., Smirnov et al., 2015). Additional model experiments would be needed to confirm the relative influence of these different processes (e.g., Zhou et al., 2014).

We acknowledge ENSO's interaction with decadal variability (e.g., via volcanic forcing Stevenson et al., 2018) and the Pacific Decadal Oscillation (PDO) inevitably plays a role modulating LM ENSO variability in the LMR (e.g., Newman et al., 2003). Preliminary analysis suggests our results are consistent (teleconnections are enhanced in the LIA) after filtering out decadal variability (applying a 2–8 year bandpass filter, Figure S11). Given that recent work indicates the PDO may become less predictable in a warming climate (Li et al., 2020), a more complete evaluation of the role of decadal variability in the LMR is needed in future work.

The LM and 21st century differ greatly in their mean state responses to radiative forcing. Our results suggest that ENSO teleconnections can strengthen given an El Niño-like mean state change, even in a cooler global-mean climate (as during the LIA). This provides an interesting analog for 21st century projections,

which show that a *warmer* mean climate enhances such teleconnections (Fasullo et al., 2018). In the Community Earth System Model (CESM) RCP8.5 Large Ensemble (Kay et al., 2015), mean El Niño rainfall anomalies intensify, resulting in an altered rainfall pattern comparable to LIA-MCA teleconnection changes (Figure S12). Similar to the LIA changes in rainfall observed in the LMR, CESM shows much wetter El Niño conditions in California and the Southwest by 2100, while changes in La Niña event composites are less conclusive. Eastern tropical Pacific warming and enhanced U.S. Southwest teleconnections may occur as a result of very different climate forcings. The causes for this different mean state/teleconnection relationship remain unclear: In the RCP8.5 case, greenhouse gas-induced global warming dominates by the end of the 21st century, but the LIA is a known period of relative global cooling due to increased volcanic activity (Brönnimann et al., 2019; Miller et al., 2012; Slawinska & Robock, 2018). It is possible that the intensification of El Niño teleconnections may be primarily driven by eastern tropical Pacific warming (regardless of the cause of that warming) rather than a direct response to mean global temperature change (Bonfils et al., 2015; Cai et al., 2014; Fasullo et al., 2018; Power et al., 2013), though additional idealized forcing simulations are needed to confirm this.

The strength and spatial expression of teleconnection rainfall may change in the future over North America, and could shift *independently of changes in ENSO* as a result of anthropogenic warming in the tropical Pacific (e.g., Bonfils et al., 2015; Power et al., 2013; Stevenson et al., 2012; Zheng et al., 2016). Teleconnections are predicted to strengthen (Fasullo et al., 2018) and change faster than changes in ENSO amplitude in simulations of the late 21st century (Stevenson, 2012). These shifts are important for understanding climate changes unique to the United States that occur on human timescales. Further, model projections suggest that Western North America in particular will experience drier conditions moving into the 21st century (Cook et al., 2015), but little attention has been paid to the superposition of ENSO teleconnection rainfall changes on predicted mean state changes. Overall, our results suggest that changes in the specific pattern of SST anomalies (rather than changes in global mean T) are highly relevant for future rainfall and extreme climate prediction, in agreement with recent work (e.g., Patricola et al., 2019; Zhao et al., 2020). If teleconnection strength and spatial expression (rainfall and temperature anomalies) shift with background warming in the tropical Pacific, impacts will include changes in the spatial structure and recurrence heavy rainfall in the southwest and southeast United States, accompanied by changes in flooding regimes in the Mississippi and Ohio River Basins (Munoz & Dee, 2017; Simon Wang et al., 2015). This work is a first step toward constraining the sign and spatial extent of these changes across the United States, enhancing their predictability. Our results underscore the importance of reducing uncertainties in the global warming pattern and mean temperature changes in the tropical Pacific (Patricola et al., 2019), and harbor implications for the predictability of teleconnection rainfall in the United States.

Data Availability Statement

All of the data used in this analysis are publicly available via the LMR website (https://atmos.uw.edu/~hakim/lmr/LMRv2/index.html Tardif et al., 2019) and the Earth System Grid (www.earthsystemgrid.org).

Acknowledgments

This work was supported by NOAA Award NA18OAR4310427 awarded to S. Dee and P. DiNezio, and NSF-AGS 1805143 awarded to S. Stevenson. We are especially grateful to Luke Parsons, who provided fixed proxy reconstructions for sensitivity testing and gave us helpful feedback on this work (Parsons & Hakim, 2019). The authors thank Xinyue Luo for conducting preliminary validation tests for ENSO behavior in the LMR, and Julien Emile-Geay for guidance on LMR version selection. Finally, we thank Jason Smerdon for his reviews of our manuscript, which vastly improved its quality and rigor, and an anonymous reviewer for their helpful comments.

References

Abram, N. J., Wright, N. M., Ellis, B., Dixon, B. C., Wurtzel, J. B., England, M. H., et al. (2020). Coupling of Indo-Pacific climate variability over the last millennium. *Nature*, *579*, 385–392.

Alexander, M. A., Bladé, I., Newman, M., Lanzante, J. R., Lau, N.-C., & Scott, J. D. (2002). The atmospheric bridge: The influence of ENSO teleconnections on air-sea interaction over the global oceans. *Journal of Climate*, *15*, 2205–2231.

Anderson, D., Tardif, R., Horlick, K., Erb, M., Hakim, G., Noone, D., et al. (2019). Additions to the last millennium reanalysis multi-proxy database. *Data Science Journal*, *18*(1), 2.

Ault, T. R., St. George, S., Smerdon, J. E., Coats, S., Mankin, J. S., Carrillo, C. M., et al. (2018). A robust null hypothesis for the potential causes of megadrought in western North America. *Journal of Climate*, *31*(1), 3–24.

Bonfils, C. J. W., Santer, B. D., Phillips, T. J., Marvel, K., Leung, L. R., Doutriaux, C., & Capotondi, A. (2015). Relative contributions of mean-state shifts and ENSO-driven variability to precipitation changes in a warming climate. *Journal of Climate*, *28*(24), 9997–10,013.

Brönnimann, S., Franke, J., Breitenmoser, P. D., Hakim, G., Goosse, H., Widmann, M., et al. (2013). Transient state estimation in paleoclimatology using data assimilation. *PAGES News*, *21*(2), 74–75.

Brönnimann, S., Franke, J., Nussbaumer, S. U., Zumbühl, H. J., Steiner, D., Trachsel, M., et al. (2019). Last phase of the Little Ice Age forced by volcanic eruptions. *Nature Geoscience*, *12*(8), 650–656.

Cai, W., Borlace, S., Lengaigne, M., Van Rensch, P., Collins, M., Vecchi, G., et al. (2014). Increasing frequency of extreme El Niño events due to greenhouse warming. *Nature Climate Change*, *4*(2), 111–116.

Cai, W., Santoso, A., Wang, G., Yeh, S.-W., An, S.-I., Cobb, K. M., et al. (2015). ENSO and greenhouse warming. *Nature Climate Change*, *5*(9), 849–859.

Clement, A. C., Seager, R., Cane, M. A., & Zebiak, S. E. (1996). An ocean dynamical thermostat. *Journal of Climate*, *9*(9), 2190–2196.
Coats, S., & Karnauskas, K. B. (2017). Are simulated and observed twentieth century tropical Pacific sea surface temperature trends significant relative to internal variability? *Geophysical Research Letters*, *44*, 9928–9937. https://doi.org/10.1002/2017GL074622
Coats, S., Smerdon, J. E., Cook, B. I., & Seager, R. (2013). Stationarity of the tropical Pacific teleconnection to North America in CMIP5/PMIP3 model simulations. *Geophysical Research Letters*, *40*, 4927–4932. https://doi.org/10.1002/grl.50938
Coats, S., Smerdon, J. E., Cook, B. I., Seager, R., Cook, E. R., & Anchukaitis, K. J. (2016). Internal ocean-atmosphere variability drives megadroughts in western North America. *Geophysical Research Letters*, *43*, 9886–9894. https://doi.org/10.1002/2016GL070105
Coats, S., Smerdon, J. E., Karnauskas, K. B., & Seager, R. (2016). The improbable but unexceptional occurrence of megadrought clustering in the American West during the Medieval Climate Anomaly. *Environmental Research Letters*, *11*(7), 74025.
Cobb, K. M., Charles, C. D., Cheng, H., & Edwards, R. L. (2003). El Niño/Southern Oscillation and tropical Pacific climate during the last millennium. *Nature*, *424*, 271–276.
Collins, M., An, S. I., Cai, W., Ganachaud, A., Guilyardi, E., Jin, F. F., et al. (2010). The impact of global warming on the tropical Pacific Ocean and El Niño. *Nature Geoscience*, *3*(6), 391–397.
Cook, B. I., Ault, T. R., & Smerdon, J. E. (2015). Unprecedented 21st century drought risk in the American Southwest and central plains. *Science Advances*, *1*(1), e1400082.
Cook, E. R., Seager, R., Heim, R. R., Vose, R. S., Herweijer, C., & Woodhouse, C. (2010). Megadroughts in North America: Placing IPCC projections of hydroclimatic change in a long-term palaeoclimate context. *Journal of Quaternary Science*, *25*(1), 48–61.
Cook, B. I., Smerdon, J. E., Seager, R., & Cook, E. R. (2014). Pan-continental droughts in North America over the last millennium* *Journal of Climate*, *27*(1), 383–397.
Cook, E. R., Woodhouse, C. A., Eakin, C. M., Meko, D. M., & Stahle, D. W. (2004). Long-term aridity changes in the western United States. *Science*, *306*(5698), 1015–1018.
D'Arrigo, R., Cook, E. R., Wilson, R. J., Allan, R., & Mann, M. E. (2005). On the variability of ENSO over the past six centuries. *Geophysical Research Letters*, *32*, L03711. https://doi.org/10.1029/2004GL022055
Dee, S., Steiger, N. J., Emile-Geay, J., & Hakim, G. J. (2016). On the utility of proxy system models for estimating climate states over the Common Era. *Journal of Advances in Modeling Earth Systems*, *18*, 1164–1179. https://doi.org/10.1002/2016MS000677
Dee, S. G., Cobb, K. M., Emile-Geay, J., Ault, T. R., Edwards, R. L., Cheng, H., & Charles, C. D. (2020). No consistent ENSO response to volcanic forcing over the last millennium. *Science*, *367*(6485), 1477–1481.
Deser, C., Phillips, A. S., & Alexander, M. A. (2010). Twentieth century tropical sea surface temperature trends revisited. *Geophysical Research Letters*, *37*, L10701. https://doi.org/10.1029/2010GL043321
Deser, C., Simpson, I. R., McKinnon, K. A., & Phillips, A. S. (2017). The Northern Hemisphere extratropical atmospheric circulation response to ENSO: How well do we know it and how do we evaluate models accordingly? *Journal of Climate*, *30*(13), 5059–5082.
DiNezio, P., Clement, A., & Vecchi, G. (2010). Reconciling differing views of tropical Pacific climate change. *Eos, Transactions American Geophysical Union*, *91*(16), 141–142.
DiNezio, P. N., Clement, A. C., Vecchi, G. A., Soden, B. J., Kirtman, B. P., & Lee, S.-K. (2009). Climate response of the equatorial Pacific to global warming. *Journal of Climate*, *22*(18), 4873–4892.
Emile-Geay, J., Cobb, K. M., Mann, M. E., & Wittenberg, A. T. (2013a). Estimating central equatorial Pacific SST variability over the past millennium. Part I: Methodology and validation. *Journal of Climate*, *26*(7), 2302–2328.
Emile-Geay, J., Cobb, K. M., Mann, M. E., & Wittenberg, A. T. (2013b). Estimating central equatorial Pacific SST variability over the past millennium. Part 2: Reconstructions and implications. *Journal of Climate*, *26*, 2329–2352. https://doi.org/10.1175/JCLI-D-11-00511.1
Emile-Geay, J., Cobb, K. M., Mann, M. E., & Wittenberg, A. T. (2013c). Estimating central equatorial Pacific SST variability over the past millennium. Part II: Reconstructions and uncertainties. *Journal of Climate*, *26*, 2329–2352.
Emile-Geay, J., McKay, N. P., Kaufman, D. S., Von Gunten, L., Wang, J., Anchukaitis, K. J., et al. (2017). A global multiproxy database for temperature reconstructions of the Common Era. *Scientific Data*, *4*, 170088.
Fasullo, J. T., Otto-Bliesner, B. L., & Stevenson, S. (2018). ENSO's changing influence on temperature, precipitation, and wildfire in a warming climate. *Geophysical Research Letters*, *45*, 9216–9225. https://doi.org/10.1029/2018GL079022
Franke, J., Brönnimann, S., Bhend, J., & Brugnara, Y. (2017). A monthly global paleo-reanalysis of the atmosphere from 1600 to 2005 for studying past climatic variations. *Scientific Data*, *4*, 170076.
Franke, J., Valler, V., Brönnimann, S., Neukom, R., & Jaume-Santero, F. (2020). The importance of input data quality and quantity in climate field reconstructions-results from the assimilation of various tree-ring collections. *Climate of the Past*, *16*(3), 1061–1074.
Frauen, C., Dommenget, D., Tyrrell, N., Rezny, M., & Wales, S. (2014). Analysis of the nonlinearity of El Niño–Southern Oscillation teleconnections. *Journal of Climate*, *27*(16), 6225–6244.
Garfinkel, C. I., Hurwitz, M. M., Waugh, D. W., & Butler, A. H. (2013). Are the teleconnections of central Pacific and eastern Pacific El Niño distinct in boreal wintertime? *Climate dynamics*, *41*(7-8), 1835–1852.
Goosse, H., Crespin, E., de Montety, A., Mann, M. E., Renssen, H., & Timmermann, A. (2010). Reconstructing surface temperature changes over the past 600 years using climate model simulations with data assimilation. *Journal of Geophysical Research*, *115*, D09108. https://doi.org/10.1029/2009JD012737
Goosse, H., Crespin, E., Dubinkina, S., Loutre, M.-F., Mann, M. E., Renssen, H., et al. (2012). The role of forcing and internal dynamics in explaining the "Medieval Climate Anomaly". *Climate Dynamics*, *39*(12), 2847–2866.
Graham, N., Ammann, C., Fleitmann, D., Cobb, K., & Luterbacher, J. (2011). Support for global climate reorganization during the "Medieval Climate Anomaly". *Climate Dynamics*, *37*, 1217–1245. https://doi.org/10.1007/s00382-010-0914-z
Hakim, G., Annan, J., Brönnimann, S., Crucifix, M., Edwards, T., Goosse, H., et al. (2013). Overview of data assimilation methods. *Pages News*, *21*(2), 72–73.
Hakim, G. J., Emile-Geay, J., Steig, E. J., Noone, D., Anderson, D. M., Tardif, R., et al. (2016). The last millennium climate reanalysis project: Framework and first results. *Journal of Geophysical Research: Atmospheres*, *121*, 6745–6764. https://doi.org/10.1002/2016JD024751
Held, I. M., & Soden, B. J. (2006). Robust responses of the hydrological cycle to global warming. *Journal of Climate*, *19*(21), 5686–5699.
Henke, L. M. K., Lambert, F. H., & Charman, D. J. (2017). Was the Little Ice Age more or less El Niño-like than the Medieval Climate Anomaly? Evidence from hydrological and temperature proxy data.
Hereid, K. A., Quinn, T. M., Taylor, F. W., Shen, C. C., Edwards, R. L., & Cheng, H. (2013). Coral record of reduced El Niño activity in the early 15th to middle 17th centuries. *Geology*, *41*(1), 51–54.
Herweijer, C., Seager, R., & Cook, E. R. (2006). North American droughts of the mid-to-late nineteenth century: A history, simulation and implication for Mediaeval drought. *The Holocene*, *16*, 159–171.

Herweijer, C., Seager, R., Cook, E. R., & Emile-Geay, J. (2007). North American droughts of the last millennium from a gridded network of tree-ring data. *Journal of Climate*, *20*, 1353–1376.
Hoell, A., Hoerling, M., Eischeid, J., Wolter, K., Dole, R., Perlwitz, J., et al. (2016). Does El Niño intensity matter for California precipitation? *Geophysical Research Letters*, *43*, 819–825. https://doi.org/10.1002/2015GL067102
Hoerling, M. P., Hurrell, J. W., & Xu, T. (2001). Tropical origins for recent North Atlantic climate change. *Science*, *292*(5514), 90–92.
Hoerling, M. P., & Kumar, A. (1997). Why do North American climate anomalies differ from one El Niño event to another? *Geophysical Research Letters*, *24*(9), 1059–1062.
Hoerling, M. P., Kumar, A., & Xu, T. (2001). Robustness of the nonlinear climate response to ENSO's extreme phases. *Journal of Climate*, *14*(6), 1277–1293.
Hoerling, M. P., Kumar, A., & Zhong, M. (1997). El niño, La Niña, and the nonlinearity of their teleconnections. *Journal of Climate*, *10*(8), 1769–1786.
Horel, J. D., & Wallace, J. M. (1981). Planetary-scale atmospheric phenomena associated with the Southern Oscillation. *Monthly Weather Review*, *109*(4), 813–829.
Johnson, N. C., & Xie, S.-P. (2010). Changes in the sea surface temperature threshold for tropical convection. *Nature Geoscience*, *3*(12), 842–845.
Karnauskas, K. B., Seager, R., Kaplan, A., Kushnir, Y., & Cane, M. A. (2009). Observed strengthening of the zonal sea surface temperature gradient across the equatorial Pacific Ocean. *Journal of Climate*, *22*(16), 4316–4321.
Kaufman, D. S., Schneider, D. P., McKay, N. P., Ammann, C. M., Bradley, R. S., Briffa, K. R., et al. (2009). Recent warming reverses long-term Arctic cooling. *Science*, *325*(5945), 1236–1239. http://www.sciencemag.org/content/325/5945/1236.abstract
Kay, J. E., Deser, C., Phillips, A., Mai, A., Hannay, C., Strand, G., et al. (2015). The Community Earth System Model (CESM) large ensemble project: A community resource for studying climate change in the presence of internal climate variability. *Bulletin of the American Meteorological Society*, *96*(8), 1333–1349.
Kennedy, J. J., Rayner, N. A., Smith, R. O., Parker, D. E., & Saunby, M. (2011). Reassessing biases and other uncertainties in sea surface temperature observations measured in situ since 1850: 2. Biases and homogenization. *Journal of Geophysical Research*, *116*, D14104. https://doi.org/10.1029/2010JD015220
Landrum, L., Otto-Bliesner, B. L., Wahl, E. R., Conley, A., Lawrence, P. J., Rosenbloom, N., & Teng, H. (2013). Last millennium climate and its variability in CCSM4. *Journal of Climate*, *26*(4), 1085–1111.
Lawman, A. E., Quinn, T. M., Partin, J. W., Thirumalai, K., Taylor, F. W., Wu, C.-C., et al. (2019). A century of reduced ENSO variability during the Medieval Climate Anomaly. *Paleoceanography and Paleoclimatology*, *35*, e2019PA003742.
Li, Q., Nakatsuka, T., Kawamura, K., Liu, Y., & Song, H. (2011). Hydroclimate variability in the North China plain and its link with El Niño–Southern Oscillation since 1784 AD: Insights from tree-ring cellulose δ18O. *Journal of Geophysical Research*, *116*, D22106. https://doi.org/10.1029/2011JD015987
Li, S., Wu, L., Yang, Y., Geng, T., Cai, W., Gan, B., et al. (2020). The Pacific Decadal Oscillation less predictable under greenhouse warming. *Nature Climate Change*, *10*(1), 30–34.
Li, J., Xie, S.-P., Cook, E. R., Huang, G., D'arrigo, R., Liu, F., et al. (2011). Interdecadal modulation of El Niño amplitude during the past millennium. *Nature Climate Change*, *1*(2), 114.
Lloyd, J., Guilyardi, E., & Weller, H. (2011). The role of atmosphere feedbacks during ENSO in the CMIP3 models. Part II: Using AMIP runs to understand the heat flux feedback mechanisms. *Climate Dynamics*, *37*(7-8), 1271–1292. https://doi.org/10.1007/s00382-010-0895-y
Lloyd, J., Guilyardi, E., & Weller, H. (2012). The role of atmosphere feedbacks during ENSO in the CMIP3 models. Part III: The shortwave flux feedback. *Journal of Climate*, *25*(12), 4275–4293. https://doi.org/10.1175/JCLI-D-11-00178.1
Lloyd, J., Guilyardi, E., Weller, H., & Slingo, J. (2009). The role of atmosphere feedbacks during ENSO in the CMIP3 models. *Atmospheric Science Letters*, *10*(3), 170–176. https://doi.org/10.1002/asl.227
Loisel, J., MacDonald, G. M., & Thomson, M. J. (2017). Little Ice Age climatic erraticism as an analogue for future enhanced hydroclimatic variability across the American Southwest. *PloS one*, *12*(10), e0186282.
Mann, M. E., Zhang, Z., Rutherford, S., Bradley, R. S., Hughes, M. K., Shindell, D., et al. (2009). Global signatures and dynamical origins of the Little Ice Age and Medieval Climate Anomaly. *Science*, *326*(5957), 1256–1260.
Masson-Delmotte, V., Schulz, M., Abe-Ouchi, A., Beer, J., Ganopolski, A., Rouco, J. F. G., et al. (2013). Information from paleoclimate archives, *Climate change 2013: The physical science basis. Contribution of Working Group I to the Fifth Assessment Report of the Intergovernmental Panel on Climate Change* (pp. 383–464). Cambridge, United Kingdom and New York, NY, USA: Cambridge University Press.
McGregor, S., Timmermann, A., England, M. H., Elison Timm, O., & Wittenberg, A. T. (2013). Inferred changes in variance over the past six centuries. *Climate of the Past*, *9*(5), 2269–2284. https://doi.org/10.5194/cp-9-2269-2013
Miller, G. H., Geirsdóttir, A., Zhong, Y., Larsen, D. J., Otto-Bliesner, B. L., Holland, M. M., et al. (2012). Abrupt onset of the Little Ice Age triggered by volcanism and sustained by sea-ice/ocean feedbacks. *Geophysical Research Letters*, *39*, L02708. https://doi.org/10.1029/2011GL050168
Munoz, S. E., & Dee, S. G. (2017). El Niño increases the risk of lower mississippi river flooding. *Scientific Reports*, *7*(1), 1772.
NOAA (2017). Past ENSO events.
Newman, M., Compo, G. P., & Alexander, M. A. (2003). ENSO-forced variability of the Pacific Decadal Oscillation. *Journal of Climate*, *16*(23), 3853–3857.
Newton, A., Thunell, R., & Stott, L. (2006). Climate and hydrographic variability in the Indo-Pacific warm pool during the last millennium. *Geophysical Research Letters*, *33*, L19710. 10.1029/2006GL027234.
PAGES2K Consortium (2013). Continental-scale temperature variability during the past two millennia. *Nature Geoscience*, *6*(5), 339–346. https://doi.org/10.1038/ngeo1797
Parsons, L. A., & Hakim, G. J. (2019). Local regions associated with interdecadal global temperature variability in the last millennium reanalysis and CMIP5 models. *Journal of Geophysical Research: Atmospheres*, *124*, 9905–9917. https://doi.org/10.1029/2019JD030426
Patricola, C. M., O'Brien, J. P., Risser, M. D., Rhoades, A. M., O'Brien, T. A., Ullrich, P. A., et al. (2019). Maximizing ENSO as a source of western US hydroclimate predictability. *Climate Dynamics*, *54*, 351–372.
Percival, D. B., & Walden, A. T. (1993). Spectral analysis for physical applications: Multitaper and conventional univariate techniques, (Vol. *154*, pp. 351–372). Cambridge University Press. https://doi.org/10.1017/CBO9780511622762
Philander, S. G. (1989). El Niño, La Niña, and the southern oscillation. *International Geophysics Series*, *46*, X-289.
Phipps, S. J., McGregor, H. V., Gergis, J., Gallant, A. J. E., Neukom, R., Stevenson, S., et al. (2013). Paleoclimate data–model comparison and the role of climate forcings over the past 1500 years*. *Journal of Climate*, *26*(18), 6915–6936.

Power, S., Delage, F., Chung, C., Kociuba, G., & Keay, K. (2013). Robust twenty-first-century projections of El Niño and related precipitation variability. *Nature*, *502*(7472), 541.
Rasmusson, E. M., & Carpenter, T. H. (1982). Variations in tropical sea surface temperature and surface wind fields associated with the Southern Oscillation/El Niño. *Monthly Weather Review*, *110*(5), 354–384.
Rasmusson, E. M., & Wallace, J. M. (1983). Meteorological aspects of the El Nino/Southern Oscillation. *Science*, *222*(4629), 1195–1202.
Ropelewski, C. F., & Halpert, M. S. (1986). North American precipitation and temperature patterns associated with the El Niño/Southern Oscillation (ENSO). *Monthly Weather Review*, *114*(12), 2352–2362.
Russon, T., Tudhope, A. W., Collins, M., & Hegerl, G. C. (2015). Inferring changes in ENSO amplitude from the variance of proxy records. *Geophysical Research Letters*, *42*, 1197–1204. https://doi.org/10.1002/2014GL062331
Rustic, G. T., Koutavas, A., Marchitto, T. M., & Linsley, B. K. (2015). Dynamical excitation of the tropical Pacific Ocean and ENSO variability by Little Ice Age cooling. *Science*, *350*(6267), 1537–1541.
Seager, R., Burgman, R., Kushnir, Y., Clement, A., Cook, E., Naik, N., & Miller, J. (2008). Tropical Pacific forcing of North American medieval megadroughts: Testing the concept with an atmosphere model forced by coral-reconstructed SSTs* *Journal of Climate*, *21*(23), 6175–6190.
Seager, R., Cane, M., Henderson, N., Lee, D.-E., Abernathey, R., & Zhang, H. (2019). Strengthening tropical Pacific zonal sea surface temperature gradient consistent with rising greenhouse gases. *Nature Climate Change*, *9*(7), 517–522.
Seager, R., Graham, N. E., Herweijer, C., Gordon, A. L., Kushnir, Y., & Cook, E. R. (2007). Blueprints for medieval hydroclimate. *Quaternary Science Reviews*, *26*, 2322–2336.
Seager, R., Harnik, N., Kushnir, Y., Robinson, W., & Miller, J. (2003). Mechanisms of hemispherically symmetric climate variability. *Journal of Climate*, *16*(18), 2960–2978.
Simon Wang, S.-Y., Huang, W.-R., Hsu, H.-H., & Gillies, R. R. (2015). Role of the strengthened El Niño teleconnection in the may 2015 floods over the Southern Great Plains. *Geophysical Research Letters*, *42*, 8140–8146. https://doi.org/10.1002/2015GL065211
Slawinska, J., & Robock, A. (2018). Impact of volcanic eruptions on decadal to centennial fluctuations of arctic sea ice extent during the last millennium and on initiation of the Little Ice Age. *Journal of Climate*, *31*(6), 2145–2167.
Smerdon, J. E., Coats, S., & Ault, T. R. (2016). Model-dependent spatial skill in pseudoproxy experiments testing climate field reconstruction methods for the Common Era. *Climate Dynamics*, *46*(5-6), 1921–1942.
Smirnov, D., Newman, M., Alexander, M. A., Kwon, Y.-O., & Frankignoul, C. (2015). Investigating the local atmospheric response to a realistic shift in the Oyashio sea surface temperature front. *Journal of Climate*, *28*(3), 1126–1147.
Solomon, A., & Newman, M. (2012). Reconciling disparate twentieth-century Indo-Pacific Ocean temperature trends in the instrumental record. *Nature Climate Change*, *2*(9), 691–699.
Steiger, N. J., Hakim, G. J., Steig, E. J., Battisti, D. S., & Roe, G. H. (2013). Assimilation of time-averaged pseudoproxies for climate reconstruction. *Journal of Climate*, *27*(1), 426–441. https://doi.org/10.1175/JCLI-D-12-00693.1
Steiger, N. J., Hakim, G. J., Steig, E. J., Battisti, D. S., & Roe, G. H. (2014). Assimilation of time-averaged pseudoproxies for climate reconstruction. *Journal of Climate*, *27*(1), 426–441.
Steiger, N. J., Smerdon, J. E., Cook, E. R., & Cook, B. I. (2018). A reconstruction of global hydroclimate and dynamical variables over the Common Era. *Scientific data*, *5*, 180,086.
Steiger, N. J., Smerdon, J. E., Cook, B. I., Seager, R., Williams, A. P., & Cook, E. R. (2019). Oceanic and radiative forcing of medieval megadroughts in the American Southwest. *Science advances*, *5*(7), eaax0087.
Stevenson, S. L. (2012). Significant changes to ENSO strength and impacts in the twenty-first century: Results from CMIP5. *Geophysical Research Letters*, *39*, L17703. https://doi.org/10.1029/2012GL052759
Stevenson, S., Fox-Kemper, B., Jochum, M., Neale, R., Deser, C., & Meehl, G. (2012). Will there be a significant change to El Niño in the twenty-first century? *Journal of Climate*, *25*(6), 2129–2145.
Stevenson, S., Overpeck, J. T., Fasullo, J., Coats, S., Parsons, L., Otto-Bliesner, B., et al. (2018). Climate variability, volcanic forcing, and last millennium hydroclimate extremes. *Journal of Climate*, *31*(11), 4309–4327.
Stevenson, S., Timmermann, A., Chikamoto, Y., Langford, S., & DiNezio, P. (2015). Stochastically generated North American megadroughts. *Journal of Climate*, *28*(5), 1865–1880.
Tardif, R., Hakim, G. J., Perkins, W. A., Horlick, K. A., Erb, M. P., Emile-Geay, J., et al. (2019). Last millennium reanalysis with an expanded proxy database and seasonal proxy modeling. *Climate of the Past*, *15*(4), 1251–1273.
Tierney, J. E., Abram, N. J., Anchukaitis, K. J., Evans, M. N., Giry, C., Kilbourne, K. H., et al. (2015). Tropical sea surface temperatures for the past four centuries reconstructed from coral archives. *Paleoceanography*, *30*, 226–252. https://doi.org/10.1002/2014PA002717
Tierney, J. E., Haywood, A. M., Feng, R., Bhattacharya, T., & Otto-Bliesner, B. L. (2019). Pliocene warmth consistent with greenhouse gas forcing. *Geophysical Research Letters*, *46*, 9136–9144. https://doi.org/10.1029/2019GLO83802
Ting, M., & Hoerling, M. P. (1993). Dynamics of stationary wave anomalies during the 1986/87 El Nino. *Climate dynamics*, *9*(3), 147–164.
Tokinaga, H., Xie, S.-P., Deser, C., Kosaka, Y., & Okumura, Y. M. (2012). Slowdown of the Walker circulation driven by tropical Indo-Pacific warming. *Nature*, *491*(7424), 439–443.
Trenberth, K. E., Branstator, G. W., Karoly, D., Kumar, A., Lau, N.-C., & Ropelewski, C. (1998). Progress during TOGA in understanding and modeling global teleconnections associated with tropical sea surface temperatures. *Journal of Geophysical Research*, *103*(C7), 14,291–14,324.
Trouet, V., Esper, J., Graham, N. E., Baker, A., Scourse, J. D., & Frank, D. C. (2009). Persistent positive North Atlantic Oscillation mode dominated the Medieval Climate Anomaly. *Science*, *324*(5923), 78–80.
Vecchi, G. A., Clement, A., & Soden, B. J. (2008). Examining the tropical Pacific's response to global warming. *Eos, Transactions American Geophysical Union*, *89*(9), 81–83.
Vecchi, G. A., Soden, B. J., Wittenberg, A. T., Held, I. M., Leetmaa, A., & Harrison, M. J. (2006). Weakening of tropical Pacific atmospheric circulation due to anthropogenic forcing. *Nature*, *441*(7089), 73–76.
Wallace, J. M., & Gutzler, D. S. (1981). Teleconnections in the geopotential height field during the Northern Hemisphere winter. *Monthly Weather Review*, *109*(4), 784–812.
Wang, J., Emile-Geay, J., Guillot, D., McKay, N. P., & Rajaratnam, B. (2015). Fragility of reconstructed temperature patterns over the Common Era: Implications for model evaluation. *Geophysical Research Letters*, *42*, 7162–7170. https://doi.org/10.1002/2015GL065265
Wang, J., Emile-Geay, J., Guillot, D., Smerdon, J. E., & Rajaratnam, B. (2013). Evaluating climate field reconstruction techniques using improved emulations of real-world conditions. *Climate of the Past Discussions*, *9*(3), 3015–3060.
Widmann, M., Goosse, H., van der Schrier, G., Schnur, R., & Barkmeijer, J. (2010). Using data assimilation to study extratropical Northern Hemisphere climate over the last millennium. *Climate of the Past*, *6*(5), 627–644.

Wittenberg, A. T. (2009). Are historical records sufficient to constrain ENSO simulations? *Geophysical Research Letters*, *36*, L12702. https://doi.org/10.1029/2009GL038710

Xie, S.-P., Deser, C., Vecchi, G. A., Ma, J., Teng, H., & Wittenberg, A. T. (2010). Global warming pattern formation: Sea surface temperature and rainfall. *Journal of Climate*, *23*(4), 966–986.

Zhao, J., Zhan, R., & Wang, Y. (2020). Different responses of tropical cyclone tracks over the western North Pacific and North Atlantic to two distinct sea surface temperature warming patterns. *Geophysical Research Letters*, *47*, e2019GL086923. https://doi.org/10.1029/2019GL086923

Zheng, X.-T., Xie, S.-P., Lv, L.-H., & Zhou, Z.-Q. (2016). Intermodel uncertainty in ENSO amplitude change tied to Pacific Ocean warming pattern. *Journal of Climate*, *29*(20), 7265–7279.

Zhou, Z.-Q., Xie, S.-P., Zheng, X.-T., Liu, Q., & Wang, H. (2014). Global warming-induced changes in El Niño teleconnections over the North Pacific and North America. *Journal of Climate*, *27*(24), 9050–9064.